Molecular Biology of the Cell
Vol. 15, 151–161, January 2004

Myosin-Va Binds to and Mechanochemically Couples Microtubules to Actin Filaments

Tracy T. Cao,* Wakam Chang,* Sarah E. Masters,* and Mark S. Mooseker*†‡

*Departments of Molecular, Cellular, and Developmental Biology and †Cell Biology and Pathology, Yale University, New Haven, Connecticut 06520

Submitted July 18, 2003; Revised September 12, 2003; Accepted September 23, 2003
Monitoring Editor: Ted Salmon

Myosin-Va was identified as a microtubule binding protein by cosedimentation analysis in the presence of microtubules. Native myosin-Va purified from chick brain, as well as the expressed globular tail domain of this myosin, but not head domain bound to microtubule-associated protein-free microtubules. Binding of myosin-Va to microtubules was saturable and of moderately high affinity (~1:24 Myosin-Va:tubulin; K_d = 70 nM). Myosin-Va may bind to microtubules via its tail domain because microtubule-bound myosin-Va retained the ability to bind actin filaments resulting in the formation of cross-linked gels of microtubules and actin, as assessed by fluorescence and electron microscopy. In low Ca^{2+}, ATP addition induced dissolution of these gels, but not release of myosin-Va from MTs. However, in 10 μM Ca^{2+}, ATP addition resulted in the contraction of the gels into aster-like arrays. These results demonstrate that myosin-Va is a microtubule binding protein that cross-links and mechanochemically couples microtubules to actin filaments.

INTRODUCTION

Myosin-Va (Myo5a) is the best characterized of three class V myosins identified in vertebrates (Berg *et al*., 2001). Myo5a is a two-headed motor, consisting of two heavy chains and multiple light chains (reviewed in Reck-Peterson *et al*., 2000). The N-terminal half of each heavy chain consists of a head or motor domain followed by a neck domain composed of six IQ motifs, each of which binds a calmodulin light chain although chicken Myo5a also contains a pair of myosin-II essential light chains (Espindola *et al*., 2000). The C-terminal tail domain consists of a proximal dimerization stalk of largely coiled-coil forming alpha helix followed by a globular domain that has been shown to interact with numerous presumed "cargo" molecules (Reck-Peterson *et al*., 2000; Karcher *et al*., 2002; Langford, 2002). The tail domain also contains at least a pair of the low-molecular-weight light chain, LC8 or PIN, first identified as a light chain of the microtuble (MT) motor, dynein, but subsequently shown to interact with numerous other proteins (Espindola *et al*., 2000). Biochemical studies on both tissue-purified and baculovirus-expressed Myo5a (reviewed in Reck-Peterson *et al*., 2000; Mehta, 2001) have shown that it is a Ca^{2+}-regulated, barbed-end directed, processive motor that takes large, ~36-nm steps in a hand-overhand manner (Forkey *et al*., 2003; Yildiz *et al*., 2003) along the actin filament.

Insights into the potential functions for Myo5a have come from several lines of investigation, including identification of organelles and proteins that interact with Myo5a (Reck-Peterson *et al*., 2000; Karcher *et al*., 2002; Langford, 2002). The most powerful strategy has been the phenotypic characterization of lethal alleles of the *dilute* (Myo5a lethal mutant) mouse and cells derived from them. The *dilute* mice develop severe seizures and die within 3 wk after birth. The primary neuronal defect thought to be responsible is the absence of smooth endoplasmic reticulum (SER) within the dendritic spines of Purkinje neurons (Takagishi *et al*., 1996). Analyses of organelle movement in cultured melanocytes (Provance *et al*., 1996; Nascimento *et al*., 1997; Wu *et al*., 1997, 1998a), neurons (Bridgman, 1999), and macrophages (Al-Haddad *et al*., 2001) from the *dilute* and wild-type mice have provided evidence for a direct role for Myo5a in both organelle transport and tethering. Moreover, in all three cell types, normal organelle movement requires participation of MT based motors as well as Myo5a. Similar results have been obtained for analysis of pigment granule movement in amphibian melanocytes (Rogers and Gelfand, 1998; Rogers *et al*., 1999). The model that has emerged from these studies is that Myo5a is primarily a passenger on organelles transported by MT motors until these organelles move into either 1) regions containing both MTs and actin filaments, which results in a Myo5a-dependent inhibition of MT-based movement through a braking effect; or 2) regions free of MTs but rich in actin (such as the dendritic processes of melanocytes) where the organelle is either moved along or tethered to actin filaments via Myo5a. The demonstration that the tail domain of Myo5a interacts with a kinesin (Huang *et al*., 1999) suggests that Myo5a may be a component of a multiprotein motor complex that provides "all cytoskeleton drive" for movement of organelles.

Although the preponderance of evidence has implicated Myo5a in organelle transport, there is also considerable evidence that this motor can interact directly with both intermediate filaments (IFs) and MTs. Recent studies have shown that Myo5a binds directly to neuronal IFs and that Myo5a is required for proper IF organization (Rao *et al*., 2002). There are also several sets of observations suggest that Myo5a may interact directly with MTs. Localization studies of Myo5a in neurons indicates substantial codistribution with MTs within the axon with both punctate (presumably organellar) and colinear staining patterns observed (Espre-

Article published online ahead of print. Mol. Biol. Cell 10.1091/mbc.E03–07–0504. Article and publication date are available at www.molbiolcell.org/cgi/doi/10.1091/mbc.E03–07–0504.

‡ Corresponding author. E-mail address: mark.mooseker@yale.edu.

Abbreviations used: IF, intermediate filament; MAP, microtubule-associated protein; MT, microtubule; Myo5a, myosin-Va.

afico *et al*., 1992; Evans *et al*., 1997; Suter *et al*., 2000). Myo5a colocalization with MTs of the centrosome as well as mitotic spindle in dividing cells has been reported for numerous types of cultured cells (Espreafico *et al*., 1998; Wu *et al*., 1998a,b; Lionne *et al*., 2001). In *Xenopus* egg extracts, an immunogen reactive with antibodies to Myo5a colocalizes with coaligned actin and MTs, implicating a role for this motor in linking the two filament systems (Waterman-Storer *et al*., 2000; Rodriguez *et al*., 2003). In the present study, we demonstrate that Myo5a, via its globular tail domain is a MT binding protein that promotes the mechanochemically active cross-linking of actin filaments to MTs.

MATERIALS AND METHODS

Myo5a Expression Constructs and Cell Culture

Chicken brain Myo5a globular tail domain (G-Tail) (aa 1421–1830) was tagged at the N terminus with His6 (QIAGEN, Valencia, CA) and at the C terminus with the FLAG epitope (Sigma-Aldrich, St. Louis, MO). Chick Myo5a head domain (aa 1–765) was tagged at the N terminus with His6. The tagged inserts were cloned into pFASTBac-dual donor plasmid and transposed to the bacmid present in DH10Bac cells to produce recombinant bacmids (BAC-to-BAC baculovirus expression system: Invitrogen, Carlsbad, CA).

Sf9 cells were grown in suspension using serum free media (Sf-900 II; Invitrogen) at 25°C. Sf9 cells were transfected with ~5 μg of bacmid DNA and 6 μl of CellFECTIN reagent (Invitrogen) to produce baculoviruses. Culture supernatants were used to infect Sf9 cells for amplification of virus stocks and for protein production.

Protein Purification

Chick brain Myo5a was purified from frozen chick brains as described previously (Cheney, 1998). Myo5a G-tail and head domains were purified from baculovirus-infected Sf9 cells lysed in 50 mM Tris-HCl, pH 8.5, 5 mM β-mercaptoethanol, 100 mM KCl, 1 mM 4-(2-aminoethyl)benzenesulfonyl fluoride, 1% NP-40. Lysates were clarified at 10,000 $\times$ *g* for 10 min at 4°C and run over a Ni-NTA agarose (QIAGEN) column equilibrated with buffer A (20 mM Tris-HCl, pH 8.5, 500 mM KCl, 20 mM imidazole, 5 mM β-mercaptoethanol, 10% [vol/vol] glycerol). The column was washed sequentially with 10 volumes of buffer A, 2 volumes of buffer B (20 mM Tris-HCl, pH 8.5, 1 M KCl, 5 mM β-mercaptoethanol, 10% [vol/vol] glycerol), and 2 volumes of buffer A. Proteins were eluted with 5 volumes of buffer C (20 mM Tris-HCl, pH 8.5, 100 mM KCl, 200 mM imidazole, 5 mM β-mercaptoethanol, 10% [vol/vol] glycerol).

Microtubule-associated protein (MAP) free, phosphocellulose-purified tubulin was prepared from frozen chick brains (100 g) following the protocol described in Hyman et al. (1990). For purification of cardiac muscle myosin II, mouse hearts were homogenized with 5 volumes of high salt buffer (300 mM KCl, 150 mM K_2HPO_4, 10 mM Na_4PO_7, 1 mM $MgCl_2$, 2 mM dithiothreitol [DTT], pH 6.8) for 20 min and clarified at 150,000 $\times$ *g* for 60 min at 4°C. The supernatants were diluted $\geq$50 times with 2 mM DTT and spun at 50,000 $\times$ *g* for 20 min at 4°C to precipitate filamentous myosin. The pellet was resuspended in myosin buffer (25 mM imidazole, pH 7.4, 4 mM $MgCl_2$, 10 mM DTT, 1 mM EGTA, 300 mM KCl) and stored in 50% glycerol at −20°C. Actin was purified from chicken pectoralis muscle by the method of Spudich and Watt (1971).

Immunoblot Analysis

For immunoblot analysis, gels were transferred onto Hybond nitrocellulose membranes (Amersham Biosciences, Piscataway, NJ). Membranes were incubated with 0.2 μg/ml anti-Myo5a tail polyclonal antibody, 0.4 μg/ml anti-head polyclonal antibody, or 10 μg/ml anti β-tubulin monoclonal antibody (Clone Tub 2.1; Sigma-Aldrich) and 1:5000 dilution of peroxidase-conjugated donkey anti-mouse or donkey anti-rabbit secondary antibody (Pierce Chemical, Rockford, IL).

Cosedimentation Analysis of Myo5a-MT and Myo5a-MT-Actin Binding

Tubulin and native Myo5a and expressed Head and G-tail domains were precleared at 250,000 $\times$ *g* for 20 min at 4°C. MTs (4 mg/ml) were polymerized in the presence of 36 μM taxol (Calbiochem, La Jolla, CA) and 1 mM GTP (Sigma-Aldrich) at 37°C for 30 min. Myo5a (0.06 μM), G-tail (1.7 μM), or Head (0.4 μM) domains were incubated with MTs (3.6 μM) at room temperature for 30 min in polymerization buffer (100 mM PIPES, pH 6.6, 1 mM $MgSO_4$, 1 mM EGTA) and then sedimentated at 250,000 $\times$ *g* for 20 min. at 25°C. Supernatants were collected and pellets were resuspended in the original volumes. Supernatants and pellets were analyzed by SDS-PAGE, and gels were Coomassie stained for MT detection and immunoblotted for Myo5a, G-tail, or Head domain detection. Determination of percent Myo5a pelleted was calculated based on densitometric scans of the blots. The relative affinity of Myo5a for MAP-free MTs was performed by sedimentation of a constant concentration of taxol-stabilized MTs (2 μM tubulin; 1.2–1.3 μM MT polymer based on densitometric analysis of tubulin in the supernatant and pellet fractions) in the presence of increasing concentrations of Myo5a (maximum concentration was 0.3–0.45 μM depending on the Myo5a preparation used). After a 30-min incubation at room temperature, the MT-Myo5a mixtures were sedimented (200,000 $\times$ *g*, 20 min, 25°C), and the amount of Myo5a in the supernatant (bound) and pellet (free) fractions was determined by densitometry of Coomassie-stained gels. The data was analyzed using Tablecurve 2D software (SYSTAT, Richmond, CA) to estimate K_d and binding ratio at saturation.

For actin cosedimentation, Head domains (0.4 μM) were incubated with phalloidin-stabilized F actin (4.8 μM) for 30 min at room temperature in polymerization buffer. Before sedimentation, either 5 mM ATP or an equal volume of buffer was added to assess ATP sensitivity of actin binding. For cosedimentation experiments with both actin and MTs, Myo5a (0.06 μM) was first incubated with MTs (3 μM) in polymerization buffer for 15 min and then actin (0.4 μM) in A′ buffer was added and incubated for an additional 15 min at room temperature. After the incubation, 5 mM ATP was added for an additional 5 min. Samples were spun at 250,000 $\times$ *g* for 20 min. Supernatants and pellets were analyzed by SDS-PAGE, and gels were Coomassie stained for MT detection and immunoblotted for Myo5a, G-tail, or Head domain detection. Determination of percent Myo5a pelleted was calculated based on densitometric scans of the blots.

Fluorescence and Immunofluorescence Microscopy

Tubulin was mixed with fluorescein-labeled tubulin (Cytoskeleton, Denver, CO) at a 4:1 ratio for a final concentration of 2 mg/ml. The samples were allowed to polymerize in the presence of 18 μM taxol and 1 mM GTP at 37°C for 30 min. F-actin (0.3 mg/ml) was stabilized with 6 μg/ml Bodipy Texas-Red phallacidin (Cytoskeleton). Myo5a (0.5 μM) or Myosin II was mixed with fluorescein-labeled MTs (1.5 μM) for 15 min at 37°C. Texas-Red labeled actin (0.25 μM) was added and incubated for an additional 15 min. Samples were examined by fluorescence microscopy by using a Nikon 100$\times$ 1.4 numerical aperture objective, and images were collected using a cooled charge-coupled device camera (Princeton Instruments, Monmouth, NJ) controlled by MetaMorph software (Universal Imaging, Downingtown, PA).

For experiments with Ca^{2+} and ATP, 4 mM Ca^{2+}-EGTA buffer (11 μM free Ca^{2+}; (Nascimento *et al*., 1996) and 2 mM ATP was added to the samples. For time-lapse microscopy, an oxygen scavenging system (0.1 mg/ml glucose oxidase, 20 μg/ml catalase, and 0.25% glucose [wt/vol]) was added to the samples. To assess effects of ATP on the cross-linked gels formed in the presence of MTs, Myo5a, and actin, the coverslips were sealed on three sides and a drop of either 40 mM ATP, ATPγS, or buffer was placed on the unsealed edge to allow diffusion of nucleotide into the sample. Images were collected every 20 s after ATP addition.

For immunofluorescence, colocalization experiments with Myo5a, samples were incubated as described above, except Myo5a was incubated with Texas-Red–labeled actin or fluorescein-labeled MTs and unlabeled MTs or actin, respectively. Samples were applied to poly-L-lysine–coated coverslips, washed with phosphate-buffered saline, and blocked with 3% bovine serum albumin in phosphate-buffered saline. Myo5a was detected using 1 μg/ml anti-Myo5a tail polyclonal antibody and 1:1000 dilution of fluorescein isothiocyanate- or Alexa Fluor 594-conjugated donkey anti-rabbit secondary antibody (Molecular Probes, Eugene, OR). Coverslips were mounted on Vectastain (Vector Laboratories, Burlingame, CA).

Thin-Section Electron Microscopy

Tubulin (2 mg/ml) was polymerized in the presence of 10 μM taxol and 1 mM GTP at 37°C for 1 h before being diluted to 1 mg/ml with polymerization buffer. MTs (1.4 μM) were mixed with Myo5a (0.1 μM) or an equal volume of polymerization buffer and incubated at room temperature for 15 min. Phalloidin-stabilized F-actin (0.3 μM) were added to the samples and allowed to incubate for an additional 15 min. For samples with ATP and Ca^{2+}, 4 mM Ca^{2+}-EGTA buffer (11 μM free Ca^{2+}), and 2.5 mM ATP was added to the mixture of Myo5a with MTs and actin for 10 min. Samples were spun at 250,000 $\times$ *g* for 20 min at 25°C. Pellets were fixed in place with 2% glutaraldehyde and 0.2% tannic acid in 0.1 M $NaPO_4$ buffer, pH 7.0, for 10 min at room temperature and for an additional 50 min on ice. Pellets were washed 3 $\times$ 5-min changes of 0.1 M $NaPO_4$ buffer. Samples were postfixed in 1% OsO_4 in 0.1 M $NaPO_4$, pH 6.0, for 1 h on ice before being washed 3 $\times$ 5-min changes of cold water. Pellets were stained overnight at 4°C with 1% uranyl acetate in water, dehydrated, and embedded in Epon 812 substitute (Electron Microscopy Services, Fort Washington, PA). Thin sections were cut perpendicular to the centrifugal field so that the top through bottom of the pellets could be viewed.

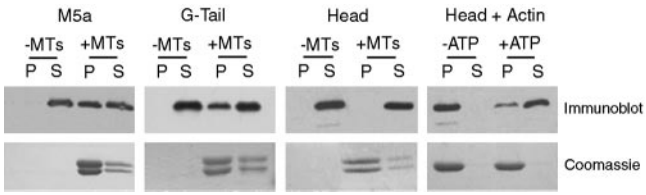

Figure 1. Myo5a binds to MTs. Sedimentation of Myo5a (0.06 μM), G-tail (1.7 μM), and Head (0.4 μM) domains in the absence (−MTs) or presence (+MTs) of taxol-stabilized MTs (3.6 μM) was performed. Content of Myo5a, G-Tail, and Head domains (top) and tubulin (bottom) in the pellet (P) and supernatant (S) fractions was assessed by immunoblot by using anti-Myo5a head or tail antibodies and Coomassie blue staining, respectively. The cosedimentation of Head domain with F-actin (4.8 μM; Head+Actin panels on right) in the absence and presence of ATP is also shown. Pellet and supernatant content of Myo5a head domain was determined by immunoblot with anti-Myo5a head antibodies and that of actin by Coomassie Blue staining.

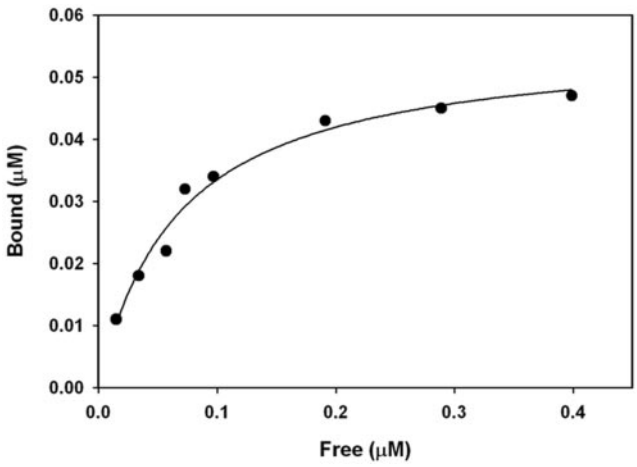

Figure 2. Sedimentation analysis of Myo5a-MT binding. Mixtures of taxol-stabilized, MAP-free MTs (1.3 μM polymer) and 0–0.45 μM Myo5a were sedimented and the concentration of Myo5a in the supernatant and pellet fractions determined by SDS-PAGE densitometry. The Myo5a binding saturates at ~1:23 M ratio with tubulin polymer and binds with an apparent K_d of ~70 nM.

RESULTS

Myo5a and Myo5a G-Tail Domains, but Not Myo5a Head Domains Interact with MTs

The binding of native Myo5a and expressed G-Tail and Head domains to polymerized, MAP-free MTs was examined by cosedimentation analysis. Both Myo5a and G-Tail, but not the Head domain partially cosedimented with MTs (Figure 1). Lack of Head domain binding was probably not due to improper protein folding of the expressed protein because it did exhibit ATP-dependent cosedimentation with actin characteristic of native Myo5a under low Ca^{2+} conditions (Nascimento *et al*., 1996). The lack of head binding to MTs, together with the observed binding of the G-tail domain suggests that the binding of native Myo5a to MTs is mediated by the tail domain with the caveat that G-tail binding may not be reflective of the binding of native, intact Myo5a. This reservation is based on the fact that G-tail also binds to tubulin dimers based on the results of affinity chromatography by using G-tail domain as affinity ligand of either crude chick brain extracts or purified tubulin dimers (our unpublished data). However, intact, native Myo5a does not bind to tubulin dimers as assessed by either sucrose velocity gradient analysis or cosedimentation of Myo5a, tubulin, and F-actin (our unpublished data).

Myo5a Binding to MTs Is Saturable and High Affinity

The affinity of Myo5a binding to MTs was assessed by cosedimentation analysis of a fixed concentration of taxol-stabilized, MAP-free MTs in the presence of increasing concentrations of native Myo5a (Figure 2). This analysis, performed using several different preparations of purified Myo5a revealed that Myo5a binding to MTs saturates at a relatively low ratio of Myo5a:tubulin polymer of ~1:22–24 with an apparent K_d of ranging from 60 to 70 nM.

Myo5a Mediates Cross-Linking of MTs to Actin Filaments

Based on the results presented above (Figure 1), the head domains of MT-bound Myo5a molecules may be free to interact with actin filaments, thus effecting a potentially important functional linkage between the MTs and actin filaments. However, given the high affinity of Myo5a for actin, binding to actin may conformationally affect the ability of Myo5a to bind to MTs. We examined the ability of Myo5a to effect the interaction of MTs with actin filaments by using a combination of fluorescence microscopy, electron microscopy (EM), and cosedimentation experiments. Fluorescence microscopy was used to examine various mixtures of MTs, actin filaments, and Myo5a by using fluorescein-labeled tubulin and Bodipy Texas-Red phallacidin-labeled F-actin. Fluorescein-labeled MTs showed as randomly distributed filaments by fluorescence microscopy (Figure 3a). MTs polymerized from these preparations of fluorescein-labeled tubulin were relatively short compared with those formed from unlabeled tubulin based on EM examination (our unpublished data). Texas-Red–labeled F-actin also seemed to be randomly distributed (Figure 3b). When Myo5a was incubated with fluorescein-labeled MTs, there was no apparent change to the distribution or appearance of the filaments (Figure 3c). As expected from previous studies (Cheney *et al*., 1993; Tauhata *et al*., 2001), when Myo5a was incubated with Texas-Red–labeled F-actin under rigor conditions, discrete bundled networks of actin filaments could be seen throughout the preparation (Figure 3d). The incubation of MTs and F-actin together did not affect the distribution or appearance of either filament (Figure 3, e–g). In contrast, when MTs were incubated with F-actin in the presence of Myo5a, large cross-linked arrays containing both MTs and actin were formed within which the MTs and actin filaments were almost completely colocalized (Figure 3, h–j)

Although this codistribution of actin and MTs in the presence of Myo5a suggests that Myo5a-dependent binding of MTs to actin has occurred, the bundling effect of Myo5a on F-actin might cause incorporation of MTs into these gel-like arrays through passive trapping. To examine this possibility, the distribution of MTs in mixtures of actin cross-linked by cardiac myosin-II thick filaments was examined. Although the arrays formed were smaller than those observed in the presence of Myo5a, many were of similar density as judged by fluorescence intensity. No trapping of MTs into the myosin-II actin networks was observed (Figure 3, k–m), indicating that the Myo5a-dependent binding of MTs to actin occurred specifically.

Under the low Ca^{2+} conditions used for these binding studies, Myo5a in solution dissociates from actin in the presence of ATP (Cheney *et al*., 1993; Nascimento *et al*., 1996; Tauhata *et al*., 2001). In contrast, Myo5a absorbed to the

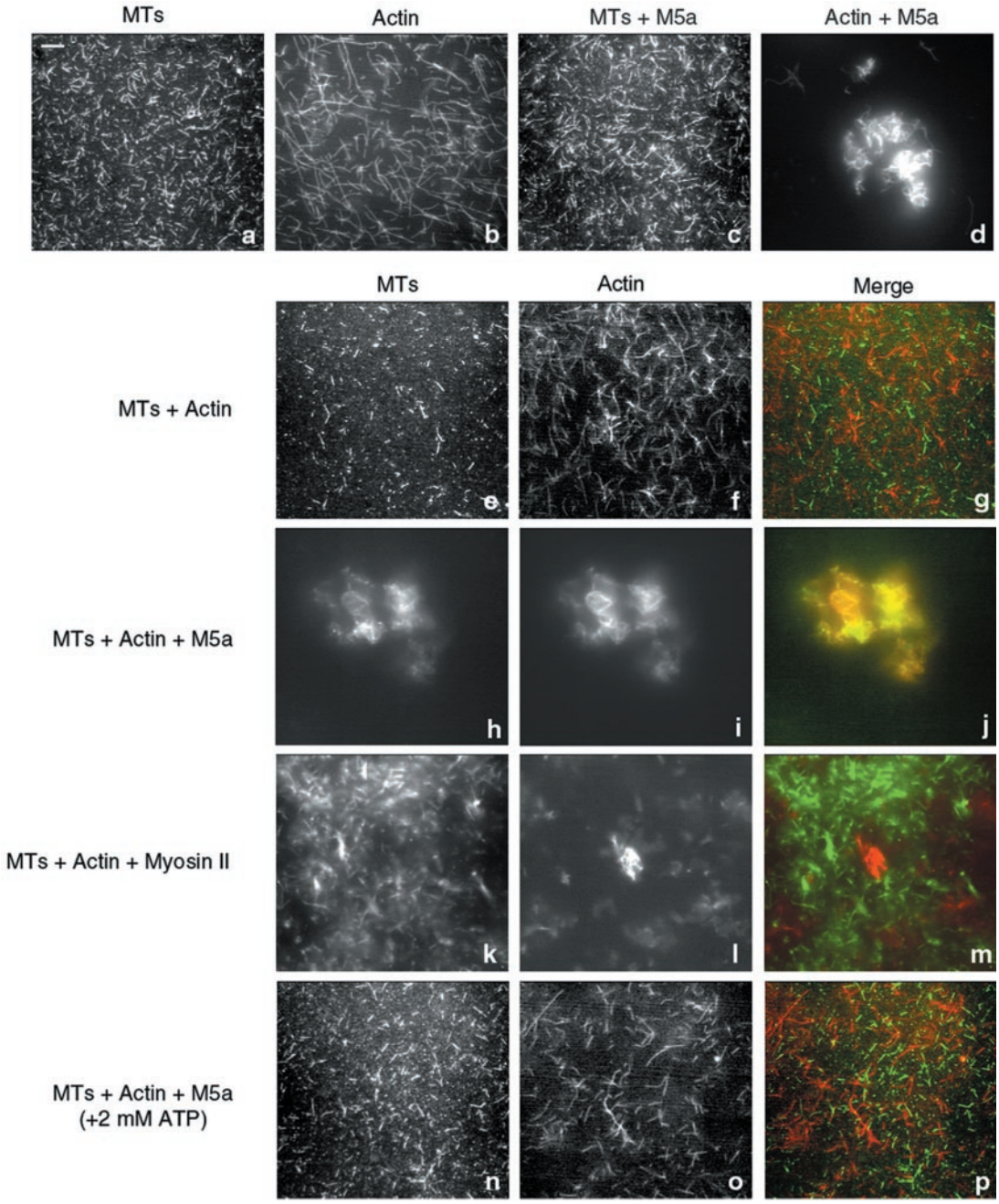

Figure 3. Myo5a-dependent cross-linking of MTs to F-actin. (a–d) Fluorescence images of fluorescein-labeled MTs (1.5 μM; a and c) and Texas Red-phalloidin–labeled F-actin (0.25 μM; b and d) in the absence (a and b) and presence (c and d) of Myo5a (0.5 μM). (e–j) Mixtures of MTs and F-actin in the absence (e–g) and presence (h–j) of Myo5a. k–m: Mixture of myosin-II-cross–linked arrays of F-actin and MTs. (n–p) Mixture of MTs, F-actin, and Myo5a in the presence of 2 mM ATP, under low Ca^{2+} conditions. The merged images show the MT signal in green and F-actin in red. Bar, 5 μm.

surface of a bead or coverglass in in vitro motility assays exhibits high-affinity actin binding in the absence of Ca^{2+} (Cheney *et al.*, 1993) suggesting that surface binding conformationally regulates the motor properties of this myosin in either a specific or nonspecific manner. Thus, it was of interest to determine whether Myo5a bound to MTs exhibited a higher affinity for actin in the presence of ATP under low Ca^{2+} conditions. This is not the case because addition of ATP results in a dissolution of the networks (Figure 3, n–p) presumably through the loss of head binding to the actin filaments in the networks. To determine whether ATP similarly affects the binding of Myo5a to MTs, cosedimentation analysis of various mixtures of Myo5a, MTs, and actin in the presence and absence of ATP was performed (Figure 4). As reported previously, the preparations of Myo5a used for these studies cosedimented with actin in the absence (M5a+A) but not presence of ATP (M5a+A+ATP). In contrast, the amount of Myo5a that cosediments in the presence of MTs is unaffected by ATP addition (Figure 4, A and B; M5a+A+MT and M5a+A+MT+ATP). Thus, Myo5a re-

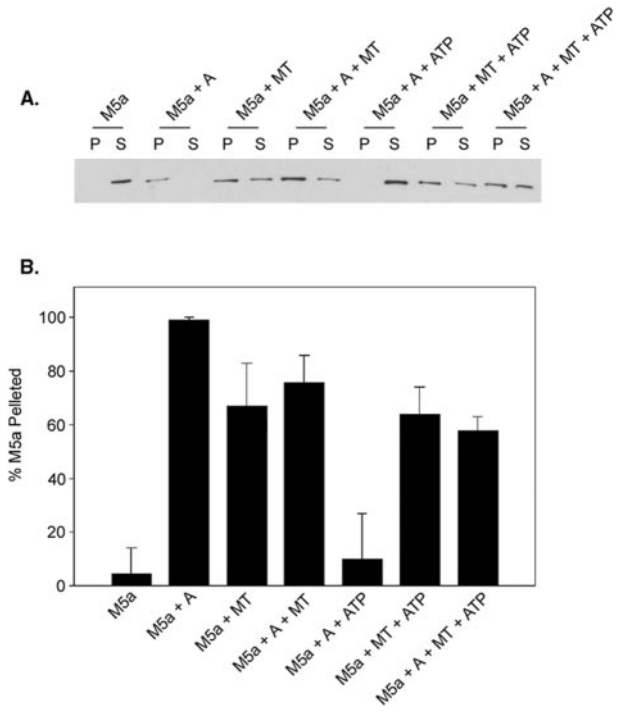

Figure 4. Sedimentation of Myo5a with MTs and F-actin in the absence and presence of ATP. (A) Anti-Myo5a immunoblot analysis of pellet and supernatant fractions after sedimentation of Myo5a (0.06 μM) alone (M5a), Myo5a and F-actin (0.4 μM) in the absence (M5a+A) and presence (M5a+A+ATP) of ATP, Myo5a and MTs (3 μM) in the absence (M5a+MT) and presence (M5a+MT+ATP) of ATP, and Myo5a, F-actin, and MTs in the absence (M5a+A+MT) and presence (M5a+A+MTs+ATP) of ATP. (B) Quantification of the amount of total Myo5a present in the pellet fraction by densitometric scans of immunoblots.

mains bound to MTs in the presence of ATP, and MT association does not affect the actin binding properties of Myo5a.

To determine the organization of the gelled networks formed by addition of actin filaments to MTs with bound Myo5a, ultrastructural analysis was performed on preparations similar in molar ratios as in Figure 3, but using untagged tubulin and actin. The gels proved to be too dense to be visualized by negative staining, and thus thin-section electron microscopy was performed on pellets collected by sedimentation of mixtures of either MTs and actin alone, or MTs with bound Myo5a and actin. In the absence of Myo5a, due to the slower sedimentation rate of actin filaments relative to MTs, the actin filaments resided almost entirely at the top of the pellet, which was devoid of MTs (Figure 5A) except for a thin zone at the interface between the two filament types (Figure 5B). Below this interface only MTs were observed (Figure 5C). As has been seen by others (Dentler and Rosenbaum, 1975; Mooseker *et al*., 1980), such pellets consist of laminar arrays of actin filaments and, further down, MTs oriented perpendicular (at all angles) to the centrifugal field. This result clearly demonstrates that there is no significant binding or trapping interactions between MTs and actin, consistent with the light microscopy analysis (Figure 3, e–g).

In contrast to mixtures of MTs and actin filaments, the pellets derived from sedimentation of MT-Myo5a-actin mixtures exhibited a strikingly different organization. Actin filaments and MTs were intermingled throughout the pellet

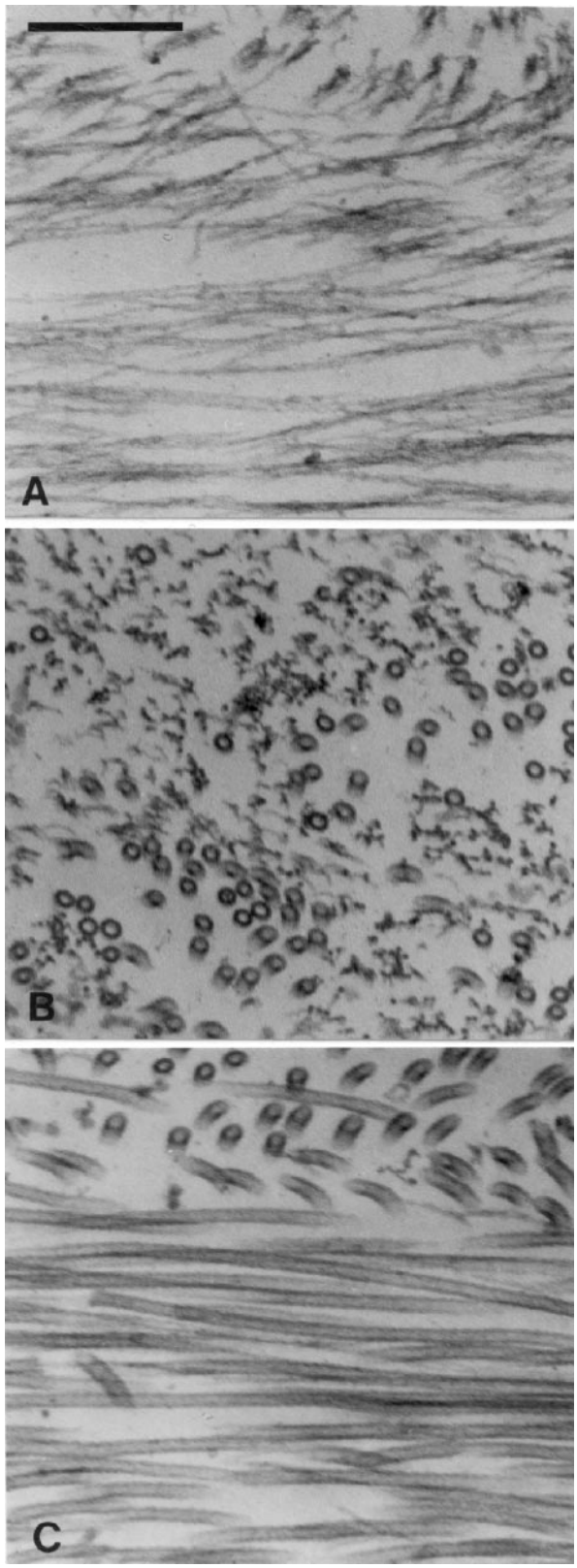

Figure 5. EM of thin sections of a pellet formed by cosedimentation of MTs (1.4 μM) and F-actin (0.3 μM). Regions near the top (A) and bottom (C) as well as the interface (B) between the layers of F-actin and MTs are shown. Note the alignment of both actin and MTs by the centrifugal field, which was roughly parallel to the vertical axis of the figure. Bar, 0.2 μm.

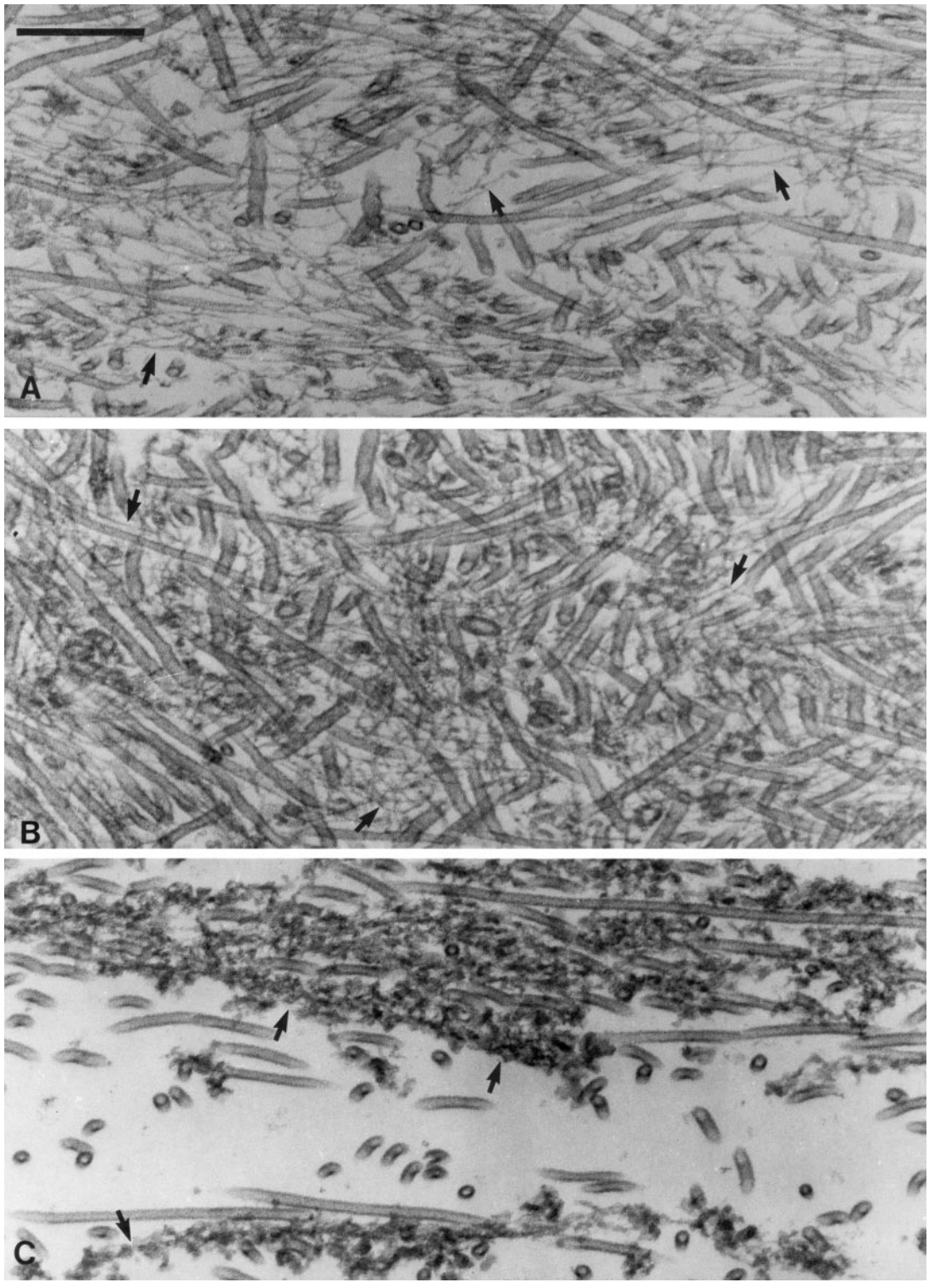

Figure 6. Thin section EM of the pellet after sedimentation of the cross-linked arrays formed by addition of F-actin (0.3 μM) to MTs (1.4 μM) with bound Myo5a (0.1 μM). As in Figure 5, images from top through the bottom (A–C) of the pellet are shown. Arrows in A and B highlight interdigitating actin filaments that are free of Myo5a along their length. Arrows in C point out actin filaments decorated along their length with Myo5a. The vertical axis of the Figure 6C is roughly aligned with the centrifugal field. Bar, 0.2 μm.

from top to bottom (Figure 6), although there was significant variability in both organization and packing density along this axis. Throughout most of the pellet, MT density was extremely high, and individual actin filaments were interdigitated between and along MTs (Figure 6, A and B). The diameter and appearance of the actin filaments in upper portion of the pellet are similar to those of naked actin filaments, suggesting that these filaments have little, if any,

bound Myo5a along their lengths (Figure 6, A and B, arrows). Another indication that there is little actin-filament-only–associated Myo5a in these regions of the pellet is that the actin is present as single filaments rather than the bundles that are formed when Myo5a is added to actin filaments under these rigor conditions (Cheney *et al*., 1993; Tauhata *et al*., 2001). Unfortunately, there are no obvious cross-linking structures discernible between MTs and actin filaments, presumably because of the low resolution of such thin-sectioned preparations. Most striking is that in the upper midportions of the pellet, both the actin filaments and MTs lay at all angles with respect to the centrifugal field, indicating that the gel strength of the cross-linked matrix was sufficiently high to withstand disruption by sedimentation. At the bottom of the pellet, MTs were more ordered by the centrifugal field. In contrast to the actin filaments in the upper regions of the pellet, the actin filaments were highly decorated with Myo5a along their lengths (Figure 6C, arrows). These decorated filaments were often present as small bundles (two to three decorated filaments, based on thickness) characteristic of the bundles formed by Myo5a at saturating ratios of Myo5a:actin (Cheney *et al*., 1993; Tauhata *et al*., 2001). These filaments presumably were formed by cooperative binding of the unbound fraction of Myo5a present when the actin filaments were added to the MT-Myo5a mixture. Although these Myo5a decorated actin filaments are intermingled with MTs, they too were oriented relative to the centrifugal field. Thus, the MTs and actin filaments at the bottom of the pellet may actually consist of those fibers that were not associated (or were released from upon sedimentation) with the MT-Myo5a-actin gel.

Calcium and ATP Induces the Contraction of Myo5a Cross-linked Networks of MTs and Actin

In the presence of ATP and micromolar levels of Ca^{2+}, Myo5a remains bound to actin and forms cross-linked arrays of filaments through intramolecular head-head cross-linking between filaments (Nascimento *et al*., 1996; Tauhata *et al*., 2001). We examined the effect of Ca^{2+} and ATP on the structure of the networks formed by Myo5a in both the absence and presence of MTs. In contrast to ATP addition in the absence of Ca^{2+}, addition of Ca^{2+} and ATP to networks formed under rigor condition did not disperse the networks. Rather, the arrays seemed much more compressed, presumably through Myo5a-mediated superprecipitation (Figure 7a). Similar compression into aster-like arrays was seen upon addition of Ca^{2+} and ATP to Myo5a cross-linked MT-actin networks (Figure 7, b–d) with most of the MT staining at the center, colocalized with the most intense actin staining. The central core of these asters was surrounded by a sphere of F-actin in which MT content was much reduced.

To assess how Myo5a is distributed within these MT-actin networks, preparations were stained with anti-Myo5a before and after addition of ATP, and its distribution compared relative to F-actin and MTs was examined. Myo5a colocalizes with both F-actin (Figure 7, e–j) and MTs (Figure 7, k–p) before (Figure 7, e–g; k–m) and after (Figure 7, h–j; n–p) ATP-induced contraction into astral arrays.

Time-lapse microscopy was used to visualize the ATP-dependent compression of bundles into aster-like structures and to verify that MTs and F-actin were coordinately redistributed (Figure 8). Images of the distribution of both MTs and actin in networks before ATP addition were taken (Start panels), and then either F-actin (Figure 8A) or MT (Figure 8B) fluorescence time-lapse images were gathered over a 100-s period, after which the microscope was refocused and images of MT and F-actin fluorescence recorded (Figure 8, End panels). In these examples, compression of both actin and MTs in these arrays began shortly after diffusing ATP into the specimen, with maximum compression generally complete within 80 s. F-actin and MTs remain codistributed within the central domain of these contracting networks throughout the process. Compared with static images of these contractile arrays (Figure 7), fluorescence intensity was reduced due to photobleaching. Moreover, the extent of contraction was less than that observed in samples to which ATP was added in suspension, either due to effects of photobleaching or adherence to the coverglass. Photobleaching was more pronounced in preparations treated with ATP compared with buffer-perfused controls (Figure 8C) in which no change in network size occurred.

Contraction of these Myo5a cross-linked arrays of MTs and F-actin required ATP hydrolysis because addition of the nonhydrolyzable ATP analog ATPγS did not induce either the dissolution or contraction of these gels (Figure 8D). This analog, which generally mimics the effects of ATP on lowering the affinity of myosins for actin does not dissociate Myo5a from F-actin in the presence of Ca^{2+} (Tauhata *et al*., 2001). Thus, in an ATP-dependent manner, Myo5a can redistribute its MT cargo via mechanochemical interaction with the actin in the array.

Ultrastructural analysis of pellets of Myo5a-cross-linked MT-actin arrays collected after treatment with ATP and Ca^{2+}, closely matched the light microscopy images (Figure 9, A and B). The pellets were biphasic with respect to MT density, consisting of dense astral-like arrays interspersed in a much less dense but still randomly ordered (relative to the centrifugal field) array of MTs, which also contained interspersed actin filaments. Within the central domain, the MTs were embedded in a densely stained meshwork comprised of Myo5a decorated actin filaments.

DISCUSSION

The central conclusions from the present study are that Myo5a is an MT binding protein and that this binding is effected by the tail domain of this motor molecule, allowing it to mechanochemically link MTs to actin filaments. Several lines of evidence support the conclusion that the tail domain effects MT binding, including the demonstration that the bacuolovirus-expressed globular tail but not head domain cosediments with MTs. However, as noted in *Results*, the binding properties of expressed G-Tail, which unlike native Myo5a binds tubulin dimers, may not be entirely reflective of the binding properties of the native motor. However, tail binding of Myo5a to MTs is also supported by the results from light microscopic and EM analyses of mixtures of MTs, Myo5a, and F-actin, (Figures 3, 5, and 6). MT-bound Myo5a retains the ability to bind to F-actin, indicating that the head domains are free. Because MT-bound Myo5a retains the ability to bind to F-actin without dissociating from the MT, this myosin cross-links MTs to F-actin, which under the in vitro conditions examined here, results into the formation of gelled arrays of MTs and actin filaments (Figures 3, 5, and 6). Finally, MT-bound Myo5a retains its characteristic ATP-dependent interactions with F-actin without dissociating from the MT as demonstrated by cosedimentation analysis (Figure 4) and the ATP-dependent dissociation of MT-Myo5a-actin gels under low Ca^{2+} conditions (Figures 3 and 4), and contraction of these gels into aster-like arrays in the presence of Ca^{2+} (Figures 7–9) .

The interaction of native Myo5a with MTs is saturable and occurs with high affinity, suggesting that Myo5a is a bona fide MAP and that MTs should be added to the ever-grow-

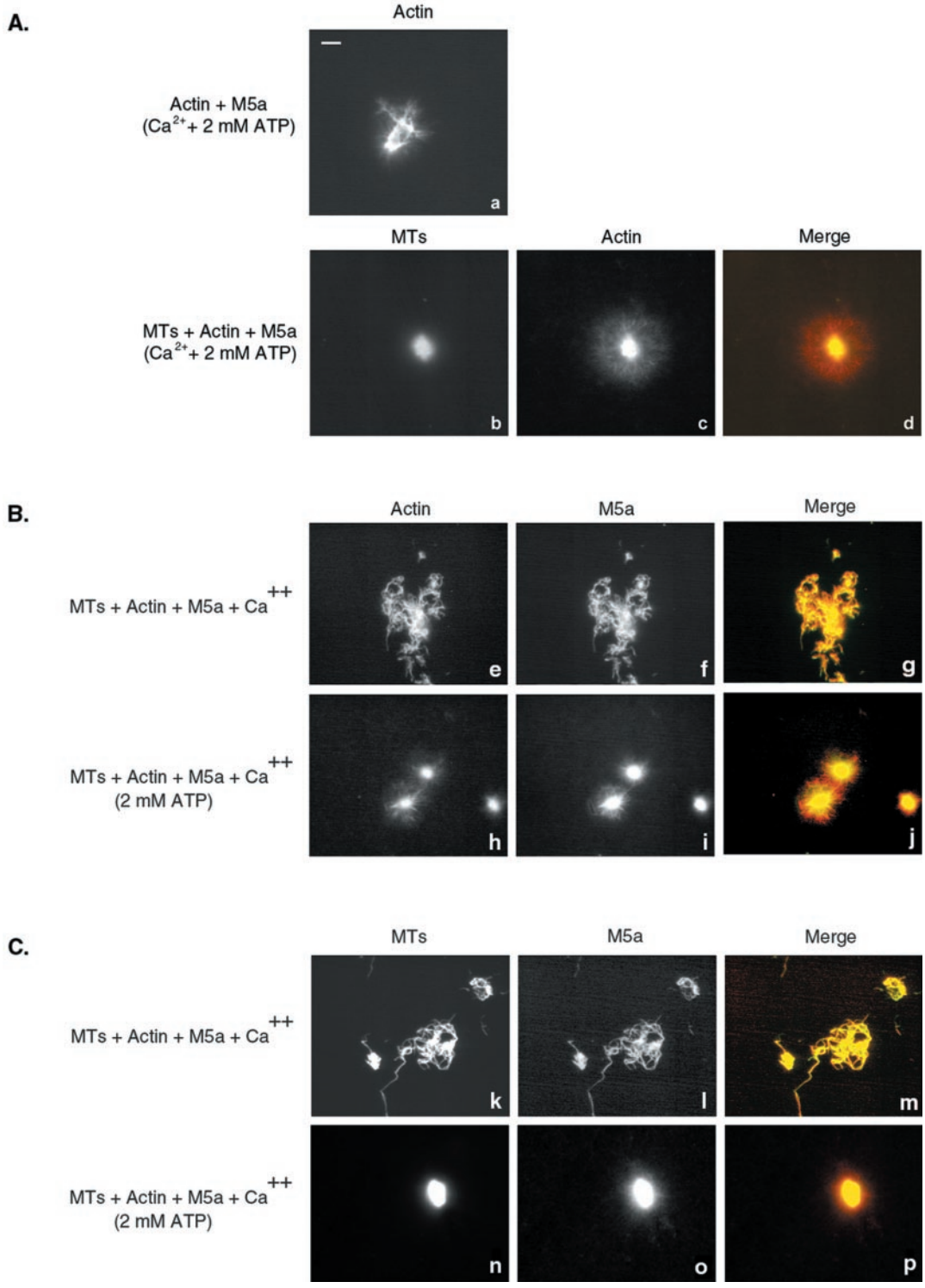

Figure 7. Myo5a-dependent contraction of MT-actin networks in the presence of Ca^{2+} and ATP. (A) Fluorescence images of actin and Myo5a (a) and mixtures of MTs, Myo5a and actin (b–d) after addition of ATP in the presence of 11 μM free Ca^{2+}. Merge image shows MT fluorescence in green and actin in red. (B and C) Immunolocalization of Myo5a with either actin (B, e–j) or MTs (C, k–p) in cross-linked arrays of MTs-Myo5a and actin in the presence of Ca^{2+} and the absence (e–g, k–m) and presence (h–j, n–p) of ATP. Bar, 5 μm.

ing list of cargos for this myosin (reviewed in Reck-Peterson *et al*., 2000; Karcher *et al*., 2002; Langford, 2002). The affinity of Myo5a for MTs (K_d = ~70 nm) is comparable with or greater than that observed for other MAPs (e.g., the MT binding domain of MAP2 [K_d = 1.1 μM, Coffey and Purich, 1995] and EMAP [K_d = 180 nm, Eichenmuller *et al*., 2001]). However, at saturation the ratio of Myo5a:tubulin is relatively low (1:22–24) compared with other MAPs such as

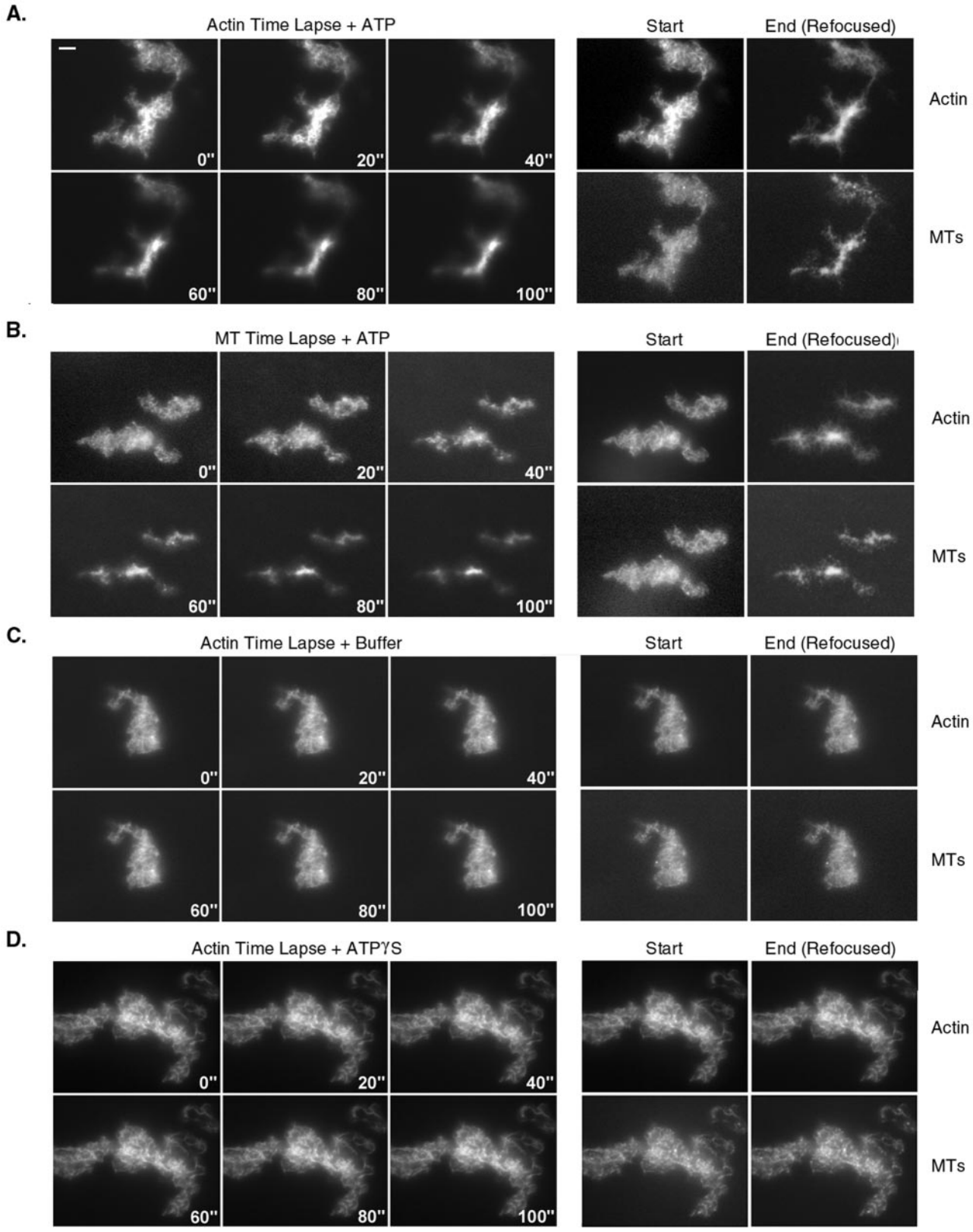

Figure 8. Time-lapse microscopy of the Ca^{2+} and ATP-dependent contraction of Myo5a cross-linked networks of MTs and actin. Visualization of either actin (A, C, and D) or MT (B) fluorescence after addition of either ATP (A and B), buffer (C) or ATPγS (D) is shown. Time in seconds after perfusion is indicated. Panels on the right show the distribution of both actin and MTs at the start and end of the time-lapse series (C). Bar, 5 μm.

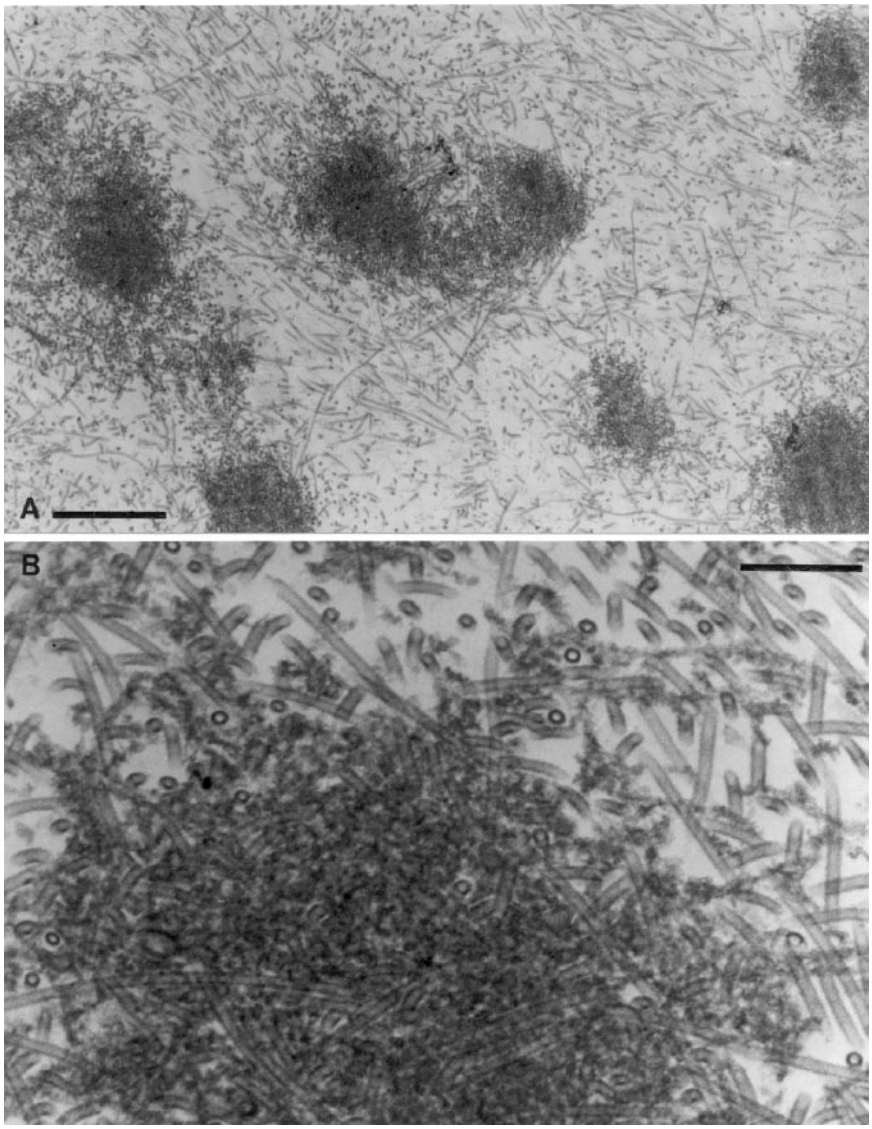

Figure 9. EM of pellet formed by sedimentation of the aster-like MT-Myo5a-actin networks after addition of Ca^{2+} and ATP. Low (A, bar, 1 μm) and high (B; bar, 0.2 μm) magnification images are shown.

MAP1A (1:15) (Pedrotti and Islam, 1994) MAP2 (1:12) (Burns and Islam, 1984), or XMAP215 (1:16) (Gard and Kirschner, 1987) that bind substoichiometrically to tubulin dimers in the MT. We were concerned that this low binding ratio might be due to the fact that only a fraction of the Myo5a present in our purified preparations exhibits MT binding activity. This is not the case, because the Myo5a present in the unbound fraction after sedimentation with MTs exhibits comparable binding to MTs added back to the initial supernatant fraction (our unpublished data). The low ratio of binding may be reflective of the fact that Myo5 is a dimer with both of the globular domains of the tail involved in binding to the wall of the MT. Unfortunately, we have had no success in our repeated attempts to visualize Myo5 along the length of MTs in negatively stained preparations. Nevertheless, given that Myo5a is a processive motor, even a single bound Myo5a motor would be sufficient to mechanochemically couple an MT to an actin filament.

Although the in vitro studies reported here demonstrate that Myo5a *can* bind directly to MTs, consideration of the numerous studies summarized in the Introduction demonstrating the colocalization of Myo5a with MTs in vivo strongly supports the idea that Myo5a *does* bind MTs in the cell. Moreover, as first suggested by the striking studies demonstrating Myo5a colocalization along MTs that serve tracks for gliding actin filaments in *Xenopus* extracts (Waterman-Storer *et al*., 2000), the results presented here demonstrate that Myo5a can mechanochemically couple MTs to F-actin. Numerous studies have illustrated the importance of the coordination between actin and MTs in a variety of cellular processes (reviewed in Gavin, 1997; Goode *et al*., 2000; Rodriguez *et al*., 2003). Myo5a may provide a critical functional link between these two cytoskeletal systems in cells in which this myosin is expressed. Moreover, it will be critical to determine whether MT binding is unique to Myo5a or is a feature of other class V myosins.

ACKNOWLEDGMENTS

This work was supported by National Institutes of Health grants DK 25387 (to M.S.M.), DK 55389 (Jon Morrow, principle investigator), and a postdoctoral fellowship from Cancer Research Fund of the Damon Runyon Walter Winchell Foundation (to T.T.C.).

REFERENCES

Al-Haddad, A., *et al*. (2001). Myosin va bound to phagosomes binds to F-actin and delays microtubule-dependent motility. Mol. Biol. Cell *12*, 2742–2755.

Berg, J.S., Powell, B.C., and Cheney, R.E. (2001). A millennial myosin census. Mol. Biol. Cell *12*, 780–794.

Bridgman, P.C. (1999). Myosin Va movements in normal and *Dilute-Lethal* axons provide support for a dual filament motor complex. J. Cell Biol. *146*, 1045–1060.

Burns, R.G., and Islam, K. (1984). Stoichiometry of microtubule-associated protein (MAP2):tubulin and the localisation of the phosphorylation and cysteine residues along the MAP2 primary sequence. Eur. J. Biochem. *141*, 599–608.

Cheney, R.E. (1998). Purification and assay of myosin V. Methods Enzymol. *298*, 3–18.

Cheney, R.E., O'Shea, M.K., Heuser, J.E., Coelho, M.V., Wolenski, J.S., Espreafico, E.M., Forscher, P., Larson, R.E., and Mooseker, M.S. (1993). Brain myosin-V is a two-headed unconventional myosin with motor activity [see comments]. Cell *75*, 13–23.

Coffey, R.L., and Purich, D.L. (1995). Non-cooperative binding of the MAP-2 microtubule-binding region to microtubules. J. Biol. Chem. *270*, 1035–1040.

Dentler, W.L., Granett, S., and Rosenbaum, J.L. (1975). Ultrastructural localization of the high molecular weight proteins associated with in vitro-assembled brain microtubules. J. Cell Biol. *65*, 237–241.

Eichenmuller, B., Ahrens, D.P., Li, Q., and Suprenant, K.A. (2001). Saturable binding of the echinoderm microtubule-associated protein (EMAP) on microtubules, but not filamentous actin or vimentin filaments. Cell Motil. Cytoskeleton *50*, 161–172.

Espindola, F.S., Suter, D.M., Partata, L.B., Cao, T., Wolenski, J.S., Cheney, R.E., King, S.M., and Mooseker, M.S. (2000). The light chain composition of chicken brain myosin-Va: calmodulin, myosin-II essential light chains, and 8-kDa dynein light chain/PIN. Cell Motil. Cytoskeleton *47*, 269–281.

Espreafico, E.M., Cheney, R.E., Matteoli, M., Nascimento, A.A., De Camilli, P.V., Larson, R.E., and Mooseker, M.S. (1992). Primary structure and cellular localization of chicken brain myosin-V (p190), an unconventional myosin with calmodulin light chains. J. Cell Biol. *119*, 1541–1557.

Espreafico, E.M., Coling, D.E., Tsakraklides, V., Krogh, K., Wolenski, J.S., Kalinec, G., and Kachar, B. (1998). Localization of myosin-V in the centrosome. Proc. Natl. Acad. Sci. USA *95*, 8636–8641.

Evans, L.L., Hammer, J., and Bridgman, P.C. (1997). Subcellular localization of myosin V in nerve growth cones and outgrowth from dilute-lethal neurons. J. Cell Sci. *110*, 439–449.

Forkey, J.N., Quinlan, M.E., Shaw, M.A., Corrie, J.E., and Goldman, Y.E. (2003). Three-dimensional structural dynamics of myosin V by single-molecule fluorescence polarization. Nature *422*, 399–404.

Gard, D.L., and Kirschner, M.W. (1987). A microtubule-associated protein from Xenopus eggs that specifically promotes assembly at the plus-end. J. Cell Biol. *105*, 2203–2215.

Gavin, R.H. (1997). Microtubule-microfilament synergy in the cytoskeleton. Int. Rev. Cytol. *173*, 207–242.

Goode, B.L., Drubin, D.G., and Barnes, G. (2000). Functional cooperation between the microtubule and actin cytoskeletons. Curr. Opin. Cell Biol. *12*, 63–71.

Huang, J.D., Brady, S.T., Richards, B.W., Stenolen, D., Resau, J.H., Copeland, N.G., and Jenkins, N.A. (1999). Direct interaction of microtubule- and actin-based transport motors [see comments]. Nature *397*, 267–270.

Hyman, A., Kellogg, D., Sawin, K.E., Wordeman, L., and Mitchison, T.J. (1990). Preparation and properties of modified tubulins. Methods Enzymol. *196*, 478–485.

Karcher, R.L., Deacon, S.W., and Gelfand, V.I. (2002). Motor-cargo interactions: the key to transport specificity. Trends Cell Biol. *12*, 21–27.

Langford, G.M. (2002). Myosin-V, a versatile motor for short-range vesicle transport. Traffic *3*, 859–865.

Lionne, C., Buss, F., Hodge, T., Ihrke, G., and Kendrick-Jones, J. (2001). Localization of myosin Va is dependent on the cytoskeletal organization in the cell. Biochem. Cell Biol. *79*, 93–106.

Mehta, A. (2001). Myosin learns to walk. J. Cell Sci. *114*, 1981–1998.

Mooseker, M.S., Graves, T.A., Wharton, K.A., Falco, N., and Howe, C.L. (1980). Regulation of microvillus structure: calcium-dependent solation and cross-linking of actin filaments in the microvilli of intestinal epithelial cells. J. Cell Biol. *87*, 809–822.

Nascimento, A.A., Amaral, R.G., Bizario, J.C., Larson, R.E., and Espreafico, E.M. (1997). Subcellular localization of myosin-V in the B16 melanoma cells, a wild-type cell line for the dilute gene. Mol. Biol. Cell *8*, 1971–1988.

Nascimento, A.A.C., Cheney, R.E., Tauhata, S.B.F., Larson, R.E., and Mooseker, M.S. (1996). Enzymatic characterization and functional domain mapping of brain myosin-V. J. Biol. Chem. *271*, 17561–17569.

Pedrotti, B., and Islam, K. (1994). Purified native microtubule associated protein MAP1A: kinetics of microtubule assembly and MAP1A/tubulin stoichiometry. Biochemistry *33*, 12463–12470.

Provance, D.W., Jr., Wei, M., Ipe, V., and Mercer, J.A. (1996). Cultured melanocytes from dilute mutant mice exhibit dendritic morphology and altered melanosome distribution. Proc. Natl. Acad. Sci. USA *93*, 14554–14558.

Rao, M.V., *et al*. (2002). Myosin Va binding to neurofilaments is essential for correct myosin Va distribution and transport and neurofilament density. J. Cell Biol. *159*, 279–290.

Reck-Peterson, S.L., Provance, D.W., Mooseker, M.S., and Mercer, J.A. (2000). Class V Myosins. Biochim. Biophys. Acta *1496*, 36–51.

Rodriguez, O.C., Schaefer, A.W., Mandato, C.A., Forscher, P., Bement, W.M., and Waterman-Storer, C.M. (2003). Conserved microtubule-actin interactions in cell movement and morphogenesis. Nat. Cell Biol. *5*, 599–609.

Rogers, S.L., and Gelfand, V.I. (1998). Myosin cooperates with microtubule motors during organelle transport in melanophores [comment]. Curr. Biol. *8*, 161–164.

Rogers, S.L., Karcher, R.L., Roland, J.T., Minin, A.A., Steffen, W., and Gelfand, V.I. (1999). Regulation of melanosome movement in the cell cycle by reversible association with myosin V. J. Cell Biol. *146*, 1265–1276.

Spudich, J.A., and Watt, S. (1971). The regulation of rabbit skeletal muscle contraction. I. Biochemical studies of the interaction of the tropomyosin-troponin complex with actin and the proteolytic fragments of myosin. J. Biol. Chem. *246*, 4866–4871.

Suter, D.M., Espindola, F.S., Lin, C.H., Forscher, P., and Mooseker, M.S. (2000). Localization of unconventional myosins V and VI in neuronal growth cones. J. Neurobiol. *42*, 370–382.

Takagishi, Y., Oda, S., Hayasaka, S., Dekker-Ohno, K., Shikata, T., Inouye, M., and Yamamura, H. (1996). The dilute-lethal (dl) gene attacks a Ca2+ store in the dendritic spine of Purkinje cells in mice. Neurosci. Lett. *215*, 169–172.

Tauhata, S.B., dos Santos, D.V., Taylor, E.W., Mooseker, M.S., and Larson, R.E. (2001). High affinity binding of brain myosin-Va to F-actin induced by calcium in the presence of ATP. J. Biol. Chem. *276*, 39812–39818.

Waterman-Storer, C., Duey, D.Y., Weber, K.L., Keech, J., Cheney, R.E., Salmon, E.D., and Bement, W.M. (2000). Microtubules remodel actomyosin networks in Xenopus egg extracts via two mechanisms of F-actin transport. J. Cell Biol. *150*, 361–376.

Wu, X., Bowers, B., Rao, K., Wei, Q., and Hammer, J.A. (1998a). Visualization of Melanosome Dynamics within Wild-Type and Dilute Melanocytes Suggests a Paradigm for Myosin V Function In Vivo. J. Cell Biol. *143*, 1899–1918.

Wu, X., Bowers, B., Wei, Q., Kocher, B., and Hammer, J.A. (1997). Myosin V associates with melanosomes in mouse melanocytes: evidence that myosin V is an organelle motor. J. Cell Sci. *110*, 847–859.

Wu, X., Kocher, B., Wei, Q., and Hammer, J.A., 3rd. (1998b). Myosin Va associates with microtubule-rich domains in both interphase and dividing cells. Cell Motil. Cytoskeleton *40*, 286–303.

Yildiz, A., Forkey, J.N., McKinney, S.A., Ha, T., Goldman, Y.E., and Selvin, P.R. (2003). Myosin V walks hand-over-hand: single fluorophore imaging with 1.5-nm localization. Science *300*, 2061–2065.